# A NEW METHOD TO DETERMINE CRITICAL GAS SATURATION AND RELATIVE PERMEABILITY DURING DEPRESSURIZATION IN THE NEAR-WELLBORE REGION

P. Egermann, O. Vizika
Institut Français du Pétrole

## ABSTRACT

Depressurization of a virgin or waterflooded oil reservoir results in the appearance of a solution gas saturation. Above a saturation threshold, this gas becomes mobile and can be produced. Knowledge of the critical gas saturation ($S_{gc}$) and the subsequent relative permeabilities ($K_r$) in the far field and the near-wellbore region has a tremendous impact on gas and oil production forecasts.

The present paper provides a new methodology to obtain representative $K_r$ and $S_{gc}$ values for a depressurization process. Specific experiments are presented in which under-saturated oil was injected upstream at a fixed rate whereas downstream the pressure was controlled in order to reproduce a drawdown. Evolution of pressure was recorded and in-situ gas saturations measured by CT-scanner. Two initial conditions were considered, fully oil saturated and at irreducible water saturation. Influence of the drawdown scheme was also explored. Transient evolution of the gas saturation profile in the core is clearly shown. Kr are deduced from history matching. They are finally compared to the $K_r$ derived from gas injection experiments.

It is demonstrated that gas/oil $K_r$ shape is strongly affected by the way the gas appears and is distributed in the porous medium. For solution gas drive, oil relative permeability is higher and gas relative permeability is smaller than for gas injection.
Concerning critical gas saturation, the experiments show two types of gas mobility depending on the operational conditions: mobility threshold attained from connection of bubbles or from mobilization of a population of separate bubbles. For the first type, $S_{gc}$ can be linked to the values obtained through static experiments at fixed depletion rate.

## INTRODUCTION

Work on depressurization has been conducted for several decades, first to study the solution gas drive as a primary recovery mechanism [1,2,3]. Recently this subject has regained interest as a good opportunity to extend life of waterflooded reservoir in the North Sea (Brent field) [4,5]. The main goal of the last researches is to optimize hydrocarbon recovery in terms of remaining gas and additional produced oil [6,7,8]. Whatever the context, primary recovery or waterflooded reservoir, it is of great importance to determine representative values of $S_{gc}$ and $K_r$ in the near wellbore region and the far field to establish reliable production forecasts. Indeed, their impact is direct on the field development, the operations planning and the sizing of surface facilities.

Most of the published results were related to the evaluation of the critical gas saturation when gas starts mobilizing [3,6,7,8]. Determination was achieved through specific experiments conducted at fixed depletion rate. Core is saturated with oil above the bubble point at secondary or tertiary condition. Then, pressure is progressively dropped at fixed rate. When gas starts flowing outside, it is considered that critical saturation is reached. As the rate applied in the laboratory is much larger than the rates effectively encountered on the field, $S_{gc}$ values for field simulations are derived by extrapolation. Concerning $K_r$, reservoir engineers usually use curves derived from gas injection experiments. However, their representativity is questionable because gas distributions, resulting from gas injection and solution gas drive, are fundamentally different. Grattoni et al showed that very low values of $K_{rg}$ are obtained when solution gas is released from waterflooded reservoir [9]. Betata et al also showed that $K_{ro}$ was strongly affected by bubble population properties contained in the porous medium [10].

Schematically, the reservoir can be divided in two parts depending of the distance from the well. In the far field, convection can be neglected so that when gas appears from solution, flow behavior is mainly controlled by $S_{gc}$. In this region, experiments at fixed depletion rate are fully representative because convection can be neglected. On the contrary, fluid velocity increases a lot in the near wellbore region and makes $K_r$ become a key parameter in terms of productivity. In addition to $S_{gc}$, it is then essential to know $K_r$ value in this area of the field. This paper proposes a new methodology to determine at the same time representative values for both parameters in the near wellbore region. Experimental apparatus and procedure is first presented. Then, measured data are provided and interpreted through numerical simulations. Permeabilities and $S_{gc}$ values are discussed at the end.

## EXPERIMENTAL APPROACH

### Rock/fluid system

All the experiments were performed on a Palatinat sandstone core whose main properties are gathered in the table below. This choice was mainly motivated by the high degree of homogeneity of this sandstone and also by its low absolute permeability.

| Permeability mD | Porosity % | Length cm | Diameter cm | $\bar{r}$ µm | PV $cm^3$ |
|---|---|---|---|---|---|
| 3.2 | 20 | 38 | 3.42 | 0.35 | 70 |

***Table 1**: Palatinat sandstone core properties*

A binary mixture $C_1C_7$ was used for the oleic phase. Depending on the experiments, bubble point ranged between 64 to 81.5 bars which corresponds to molar fraction of $C_1$ of 0.295 and 0.358. The table hereafter provides the associated properties in terms of IFT and viscosity. Data were derived from IFP developed PVT software.

| Pb bars | % C1 molar | IFT mN/m | Viscosity cP |
|---|---|---|---|
| 81.5 | 35.8 | 8.52 | 0.271 |
| 64 | 29.5 | 10.78 | 0.308 |

***Table 2**: properties of the binary mixture $C_1C_7$*

The brine is composed of 50 g/l NaCl and 5 g/l $CaCl_2$ because it was proved to be efficient in stabilizing clays contained in the sandstone [11].

**Experimental setup**

A general description of the setup is provided on **Sketch 1**. It is mainly composed of a Hassler type core holder made with composite material, which enables acquisition of local saturation measurements along the core with CT-scanner. At the inlet, the binary mixture can be injected into the core at a fixed rate through an ISCO pump. Downstream, the outlet pressure is controlled with a PC by a regulator, so that drawdown can be monitored very easily. At the outlet, a densimeter is used mainly during the core preparation to check the core saturation with the mixture. During experiment, the densimeter is also useful to detect the very first apparition of the gas phase downstream. Fluids are collected into a separator so that both liquids and gas can be measured. Evolution of the pressure downstream is directly recorded by a pressure gauge. Inlet pressure is deduced from a differential pressure gauge measurement. As none pressure ports have been implemented along the core, the pressure profile is not available. All the data are automatically recorded on a PC.

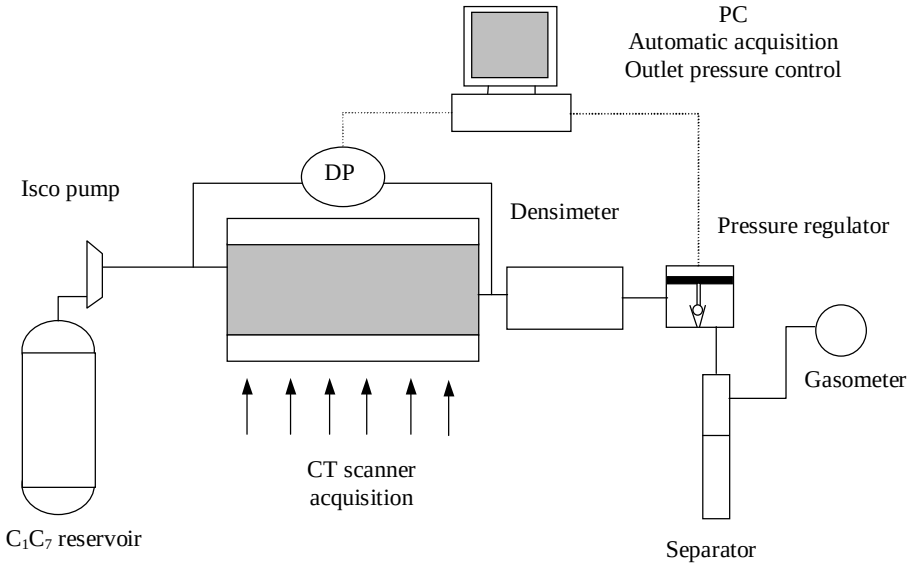


***Sketch 1**: experimental set-up*

**Initial saturation**

Experiments were performed with fully oil saturated medium and at irreducible water conditions. The core is first cleaned by injecting ethyl and isopropyl alcohol. Then, drying was realized by flooding of $CO_2$ in an oven at low temperature (40°C). The core is saturated with $C_1$ to measure one of the reference profiles required to deduce saturations from CT-scanner. Then, the core is flooded with $CO_2$ again before being saturated with $C_7$ by vacuum. The mixture is put in place by injection under pressure. At the outlet, the density value is controlled. When the signal stabilizes, it is assumed that the whole core is saturated with the mixture. Typically, this is achieved after injection of roughly 15 PV.

When irreducible water saturation is required, the core is vacuum saturated with brine. Then, Marcol 52 (10 cP) is injected until water production ceased. Marcol is pushed out by pure $C_7$ injection and finally the core is flooded with the mixture under pressure. Reference profiles are also measured when the core is fully saturated with $C_1C_7$ and water. $S_{wi}$ is calculated by mass balance and cross-checked by CT-scanner.

**Experimental procedure**

The principle of experiment was described in [11,12]. Whatever the initial saturation into the core, nature of experiments does not change. Upstream, injection of oil is performed at fixed rate with the outlet pressure first above the bubble point so that presence of gas is excluded. Pressure at the outlet is progressively decreased (10 bar/hour) to a defined value below the bubble point of the mixture. All experiments were performed with a rate of 70 cc/h to reproduce what happens in the wellbore of a production well. The drawdown caused the formation of the gas phase in the downstream part of the core. Transient evolution of gas saturation through the core is followed by CT-scanner and impact of gas apparition on the pressure drop is recorded by inlet pressure variations.

# RESULTS

Two drawdown shapes were considered for each initial saturation state (fully oil saturated and irreducible water conditions).

**Fully oil saturated**

Two experiments have been performed at fully oil saturated conditions: one with 10 bars between the downstream pressure ($P_o$) and the bubble pressure ($P_b$) and the other with only 6 bars difference. For both experiments, pressure evolutions are very similar (Figure 1). At the beginning, inlet and outlet pressures remain parallel. This part corresponds to a constant low-pressure drop along the core during the monophasic flow of oil when outlet pressure is above the bubble point. As soon as gas appears from downstream, pressure drop increases with gas saturation. As the pressure is fixed at the outlet, it makes the inlet pressure increase. For longer times, stabilization of the pressure is observed and must correspond to the establishment of a stabilized state in term of gas saturation along the core (permanent state). Mean features related to experiments are summarized in Table 3.

| | ε, bars = $P_b$- $P_o$ | $P_b$ , bars | Stabilization time | Stabilized pressure drop, bars | Saturation Jump, % |
|---|---|---|---|---|---|
| Exp 1 | 10 | 81.5 | 6 H | 13.2 | 24 |
| Exp 2 | 6 | 64 | 4.5 H | 12.9 | 17 |

***Table 3**: fully oil saturated experiments characteristics*

These observations are in good agreement with CT-scanner measurements (Figure 2). For the first experiment (ε=10 bars), three different steps can be distinguished in the transient gas saturation profiles evolution:

- The first one is related to the progression of the gas phase from downstream to upstream. The shape of the saturation profile is practically linear and should correspond roughly to the local pressure profile.
- During the second step, gas saturation profile recedes in the upstream part. This behavior is certainly associated with the particular shape of the inlet pressure. The pressure rebound related to the gas appearance pressurizes the upstream part of the core and eliminates existing, non-mobile gas by dissolution.
- The final step corresponds to the stabilization of the gas saturation profile as suggested by the upstream pressure evolution. Its shape is very particular with a high jump followed by a slight increase.

Accuracy of saturation with CT scanner is around 3% (saturation units) and explains that $S_g$ values are not exactly zero in the upstream part of the core.

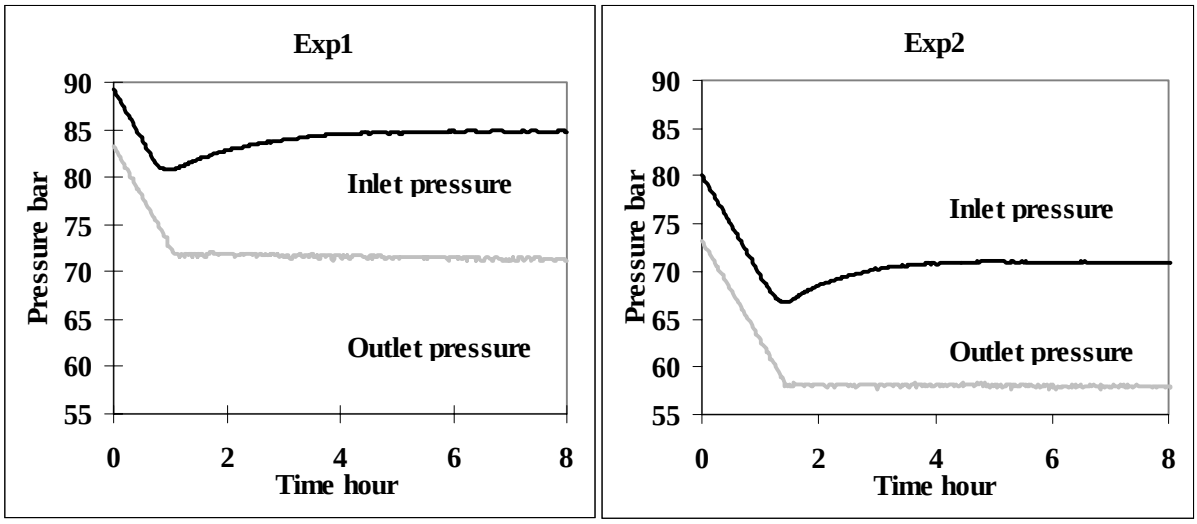


*Figure 1: evolution of inlet and outlet pressures (fully oil saturated)*

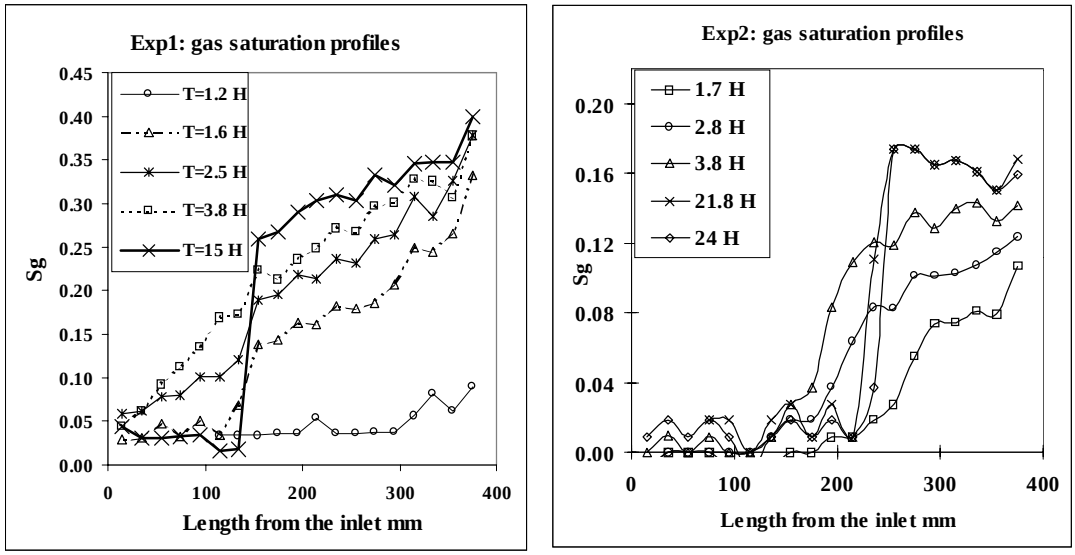


*Figure 2: evolution of gas saturation: accuracy ±3% (fully oil saturated)*

Gas saturation profiles are radically different for the second drawdown scheme (ε=6 bars). As expected, the general extension of the two-phase area is smaller since the injection rate is the same but ε is lower. For the shorter times, evolution is identical. Differences appear for longer times when profile stabilizes. A maximum value of gas saturation is observed inside the core and gas saturation decreases going downstream. These features mean that gas is not in equilibrium with oil in this case. The general decreasing shape of the gas saturation profiles is not conventional. It suggests that gas mobilization process does not rely on bubble connection but rather on dispersed bubble displacement. This assumption will be explored with numerical simulations.

**Irreducible water saturation**

Two drawdowns were also considered here. General features of experiments are gathered in Table 4. Initial CT scanner $S_{wi}$ profiles were very homogeneous in both cases. Evolution of

pressures at both ends of the core is very similar to Exp1 and Exp2 (Figure 3). Nevertheless, compared to fully oil saturated experiments, the initial monophasic pressure drop is higher since oil permeability is reduced by the presence of water ($K_{ro}@S_{wi}=0.55$). Upstream extension of the gas saturation is lower (Figure 4) because the pressure gradient is larger. Hence, only a small downstream part of the core remains under the bubble point when permanent flow is reached. This lowers the time required to stabilize the pressure response (3 hours compared to 4.5-6 for previous experiments).

| | ε, bars $=P_b-P_o$ | $P_b$ , bars | Stabilization time | Stabilized pressure drop, bars | $S_{wi}$ , % |
|---|---|---|---|---|---|
| Exp 3 | 4.5 | 67 | 3 H | 21.5 | 50 |
| Exp 4 | 4 | 74 | 2.5 H | 20.3 | 48 |

***Table 4**: irreducible water saturated experiments characteristics*

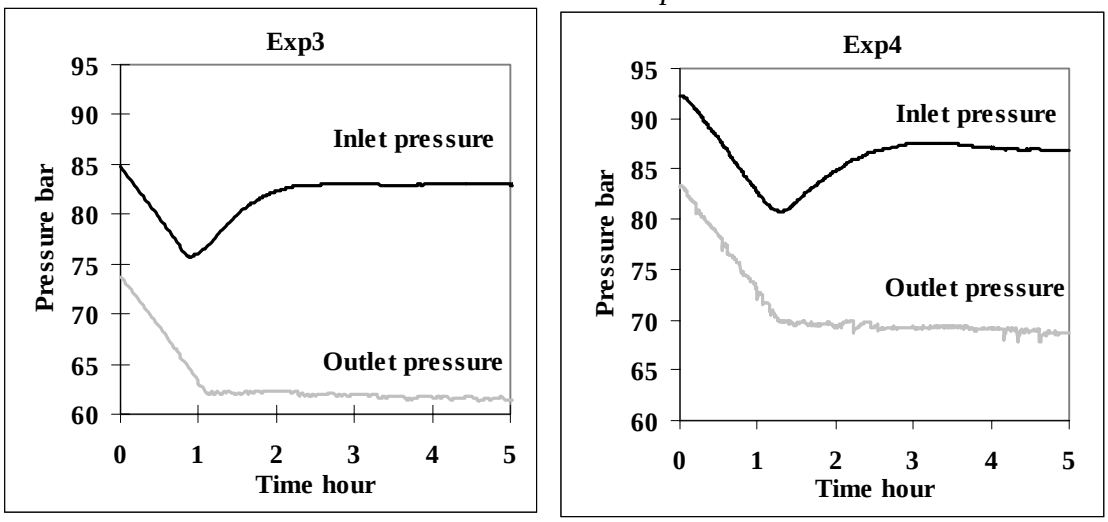


*Figure 3: evolution of inlet and outlet pressures (irreducible water conditions)*

The general shape of gas saturation profiles reminds results obtained in Exp2. Gas saturation initially increases then decreases going downstream.

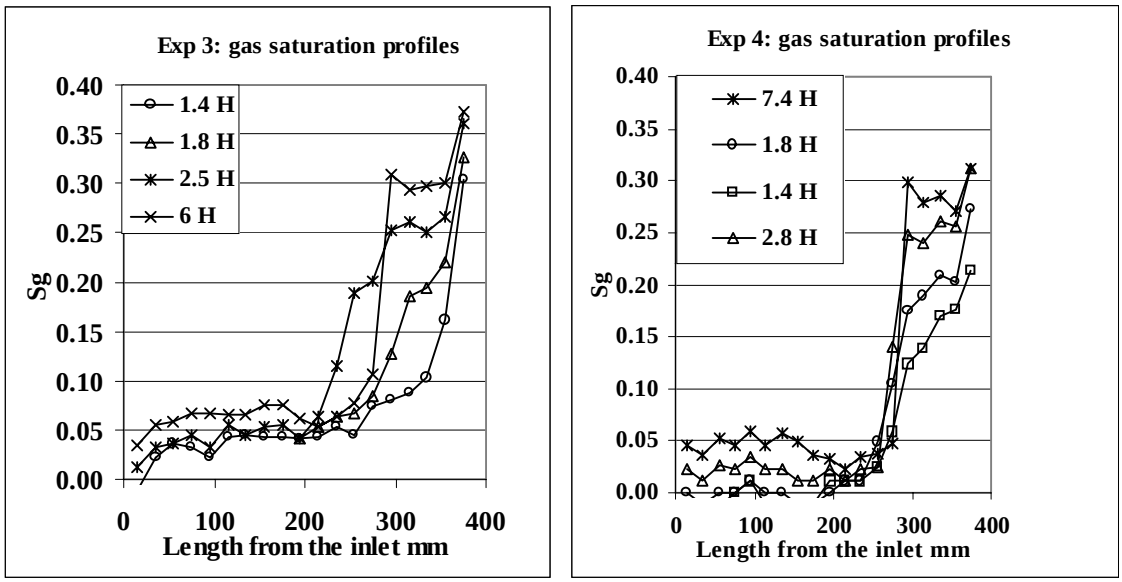


*Figure 4: evolution of gas saturation (irreducible water conditions)*

# INTERPRETATION

## Numerical simulator

Numerical interpretation of Exp1 has been possible by history matching of experimental data using a standard reservoir simulator (ATHOS), and the corresponding Kr and Sgc were deduced. The other experiments involved different physical phenomena not taken into account in a classical reservoir simulator. In order to interpret these experiments a specific numerical code was developed within this study. Compared to classical reservoir simulators, this in house code provides two main advantages. First, it enables to take into account the physical phenomena related to gas formation and growth in porous media. Hence, gas nucleation and growing of the existing bubbles by diffusion are fully implemented which permits simulator to be more accurate during the transient evolution of the gas saturation profiles. On the second hand, mobilization of the gas phase can be easily controlled. As suggested by experimental observations, two types of mobilization were implemented:

- The first one is classical and corresponds to the connection of the bubbles. Once $S_{gc}$ is reached, gas flows continuously into the connected path.
- The second one is related to a mobilization of the gas bubbles before the connection is reached. It is assumed that a bubble becomes mobile when the viscous pressure gradient is higher than the capillary forces as suggested in reference 10:

$$\left(\frac{dP}{dx}\right)_{visq} > \frac{P_c^{th}}{2r_b}$$

General structure of the code is detailed in Sketch 2. The nucleation-diffusion module was derived from an existing code developed in reference 3 and devoted to simulate static experiments at fixed depletion rate. To meet the requirements of the actual experiments, the module is included inside a dynamic loop. Pressure is first calculated along the core through Darcy's law. Then, nucleation-diffusion is activated in each cell and new gas saturation is evaluated. Depending on the gas bubble population properties and the pressure gradient, the code determines if one of the mobilization criteria is reached and transfers some gas in the adjacent cell. Oil rate and dissolute gas concentration are then updated to take into account gas mobilization.

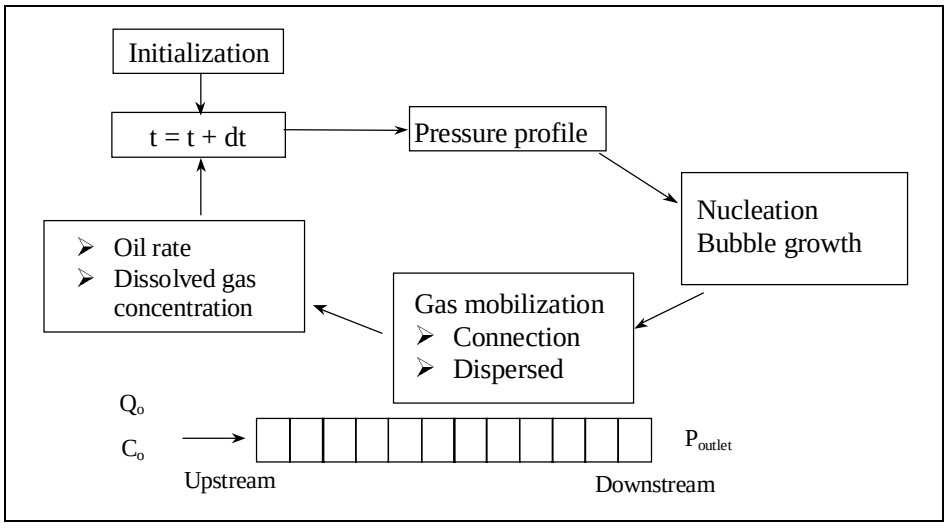


*Sketch 2: structure of the code*

**History matching of Exp1 (bubble connection)**

Figure 5 shows that an excellent agreement is obtained for inlet and outlet pressures. This trend is also confirmed with gas saturation profiles. The three steps observed in the transient evolution of $S_g$ are particularly well simulated: linear advance, regression of the gas front by dissolution and stabilization of the profile. A more accurate comparison of gas profiles is given on Figure 6 ,1.4 and 15 hours after the beginning of injection.

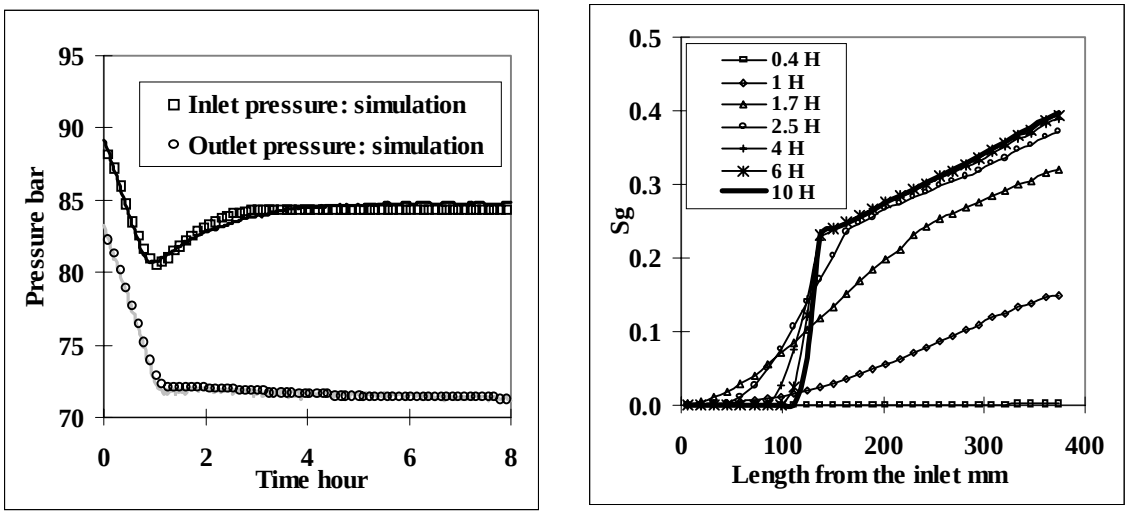


*Figure 5: history matching of Exp1*

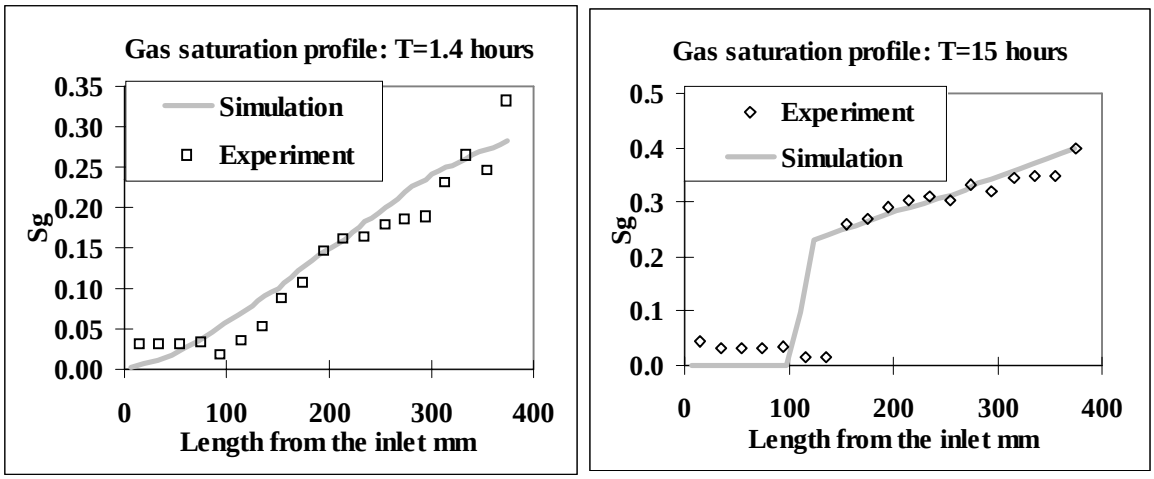


*Figure 6: Gas saturation profiles*

The fitting was reached by manual trial and error method. Fortunately, it appears from the simulations that all the parameters to be adjusted have not the same impact on data. Then, a methodology can be easily find out to shorten adjustment time:

- $S_{gc}$ is equal to the height of the gas saturation jump observed on the stabilized profile.
- $K_{ro}$ mainly affects the shape of the inlet pressure rebound and also the upstream extension of the gas stabilized profile.
- $K_{rg}$ has little impact on pressure drop and only contributes to the shape of the gas stabilized profile. The lower the $K_{rg}$, the higher is the gas saturation increase downstream the jump.

**History matching of Exp3 (dispersed phase displacement)**

Compared to Exp1, simulations show that dispersed phase displacement occurs in Exp3. Mobilization of the dispersed phase (gas) is mainly due to the pressure gradient, which is higher because of the presence of irreducible water saturation. It makes viscous forces over the largest bubbles be strong enough to mobilize them before reaching connection. Similar results were obtained with Exp2 but the origin of bubble mobilization differs. As ε was lower in Exp2 than in Exp1, nucleation was stopped early. Hence, bubble number was limited which tends to increase bubble size and viscous forces over them.

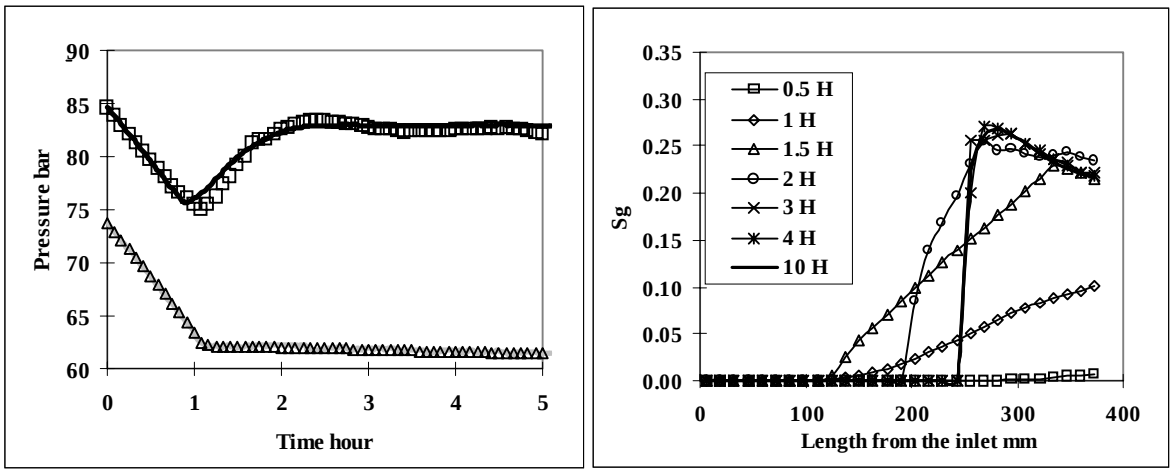


*Figure 7: history matching of Exp3*

As observed experimentally, the simulations correctly predict the decreasing gas saturation profiles towards the core outlet. The inlet pressure is also well simulated although the dispersed flow of gas brings some oscillations in the simulations. The mobilization threshold pressure was found to be equal to 0.17 bar. This value is consistent with Purcell capillary pressure curve of the Palatinat since Percolation plateau ranged between 0.13 and 0.18 bar.

# DISCUSSION

## Kr

In this part, $K_r$ obtained through Exp1 are compared with $K_r$ curves derived from gas injection experiment on companion plug (Marcol/air). It is clear from Figure 8 that both $K_{ro}$ and $K_{rg}$ depend on the process. $K_{ro}$ values are higher for solution gas drive than for gas injection. This behavior is attributed to the phase distribution differences between gas injection and solution gas drive. When gas is injected, it invades the largest pores, it is continuous and highly mobile, and, even at low saturations, it inhibits oil flow. In solution gas drive instead, gas bubbles appear next to the pore walls in all pores independently of their size. This gas is initially discontinuous and immobile and gets connected only above a often very high $S_{gc}$.

Trend is opposite with $K_{rg}$ since the curve is several orders of magnitude lower in solution gas drive experiments. Similar curves of $K_{rg}$ were obtained by Grattoni et al in tertiary conditions. They proved that gas mobility is always very low when gas comes from solution. The shape of $K_{rg}$ curve is also very particular with a jump around $S_{gc}$ followed by a slight increase.

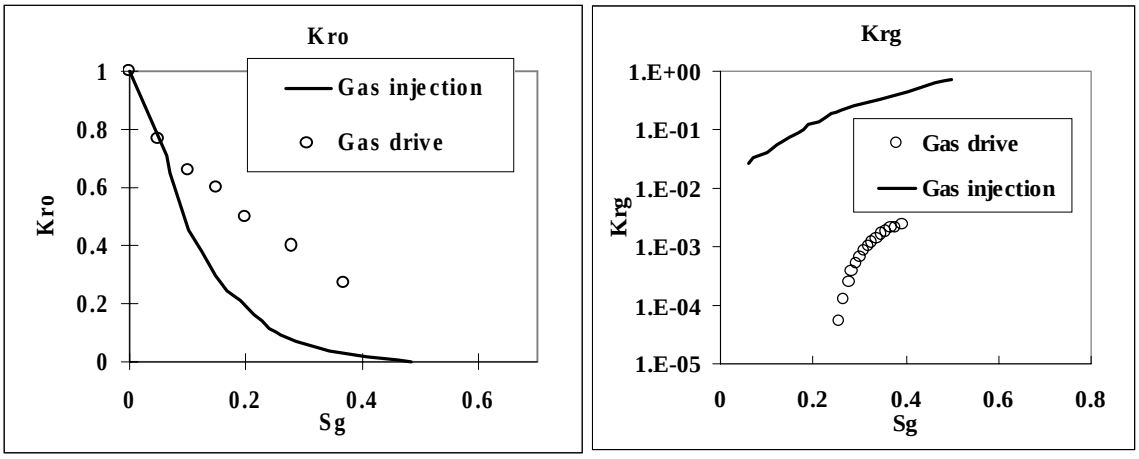


*Figure 8: comparison between gas injection and solution gas drive $K_r$ curves*

**$S_{gc}$**

Simulation of Exp1 showed that a consistent value of $S_{gc}$ could be derived from experiment (gas saturation jump). Hence, it is interesting to see how this type of value can be compared with standard method used by reservoir engineers (extrapolation in Log-Log of dP/dt function of $S_{gc}$ chart). Numerical simulations proved that oil and free gas were in quasi thermodynamic equilibrium when stabilization is reached. Same phenomenon is observed with static experiments conducted at fixed depletion rate. In both cases, the quasi steady state results from equilibrium between diffusion and supersaturation. Origin of supersaturation only differs:

- In Exp1, supersaturation comes from displacement of oil downstream in area were pressure is lower. Hence, supersaturation is fed by convection through dP/dx.
- At fixed depletion rate, supersaturation directly results from dP/dt.

This analogy suggests that a comparison of $S_{gc}$ is possible if a representative equivalent depletion rate is calculated from Exp1.

$$\frac{dP}{dt} \approx \frac{dx}{dt} \times \frac{dP}{dx} \approx U \times \frac{dP}{dx}$$

$$U = \frac{Q_o}{\phi\ A} \qquad \text{and} \qquad \frac{dP}{dx} = \frac{Q_o L \mu_o}{KA}$$

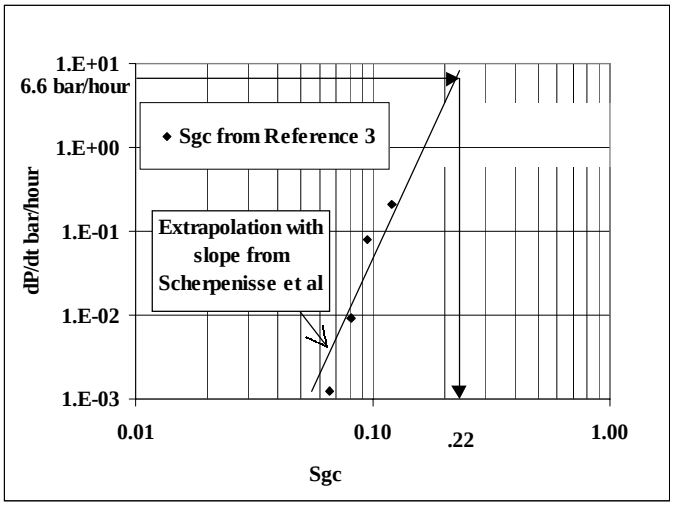


*Figure 9: Comparison of $S_{gc}$ value with routine method of extrapolation*

The numerical application gives an equivalent dP/dt equal to 6.6 bar/hour. Comparison is made on Figure 9 with experimental data derived from reference 3 because initial saturation conditions are identical and IFT of the mixture used are very close (11.5 mN/N versus 8.5 mN/m). Extrapolation was performed with the analytical slope reported by Scherpenisse et al [7]. It gives 22% for $S_{gc}$ at 6.6 bar/hour, which is almost the value found experimentally (24%). It has to be noted that correction due to IFT differences would lead to a slight translation of the extrapolation line to the right and would give higher value of the estimation.

Interpretation of experiments show that dispersed displacement of gas is possible when viscous gradient over the bubble is higher than a threshold value of capillary pressure. This displacement process occurs when bubble size is large (low $\varepsilon$) or when pressure gradient is high enough. Hence, two definitions of $S_{gc}$ have been introduced. From its definition, $S_{gc}$ resulting from dispersed displacement is always lower than the one derived from bubble connection at a given equivalent depletion rate. The difference between the two values increases with viscous gradient. This result could explain qualitatively some experimental observations made on cold production process of heavy oil [13,14]. As viscosity of such oils is around several thousands of centipoises, viscous gradient is very high in spite of favorable absolute permeability. Hence, it favors an early mobilization of gas in dispersed bubbles. This prediction is in good agreement with experimental results since low values of $S_{gc}$ have been obtained.

## CONCLUSIONS

A new methodology has permitted to determine representative values of near wellbore $K_r$ and $S_{gc}$ by history matching of experimental data. Compared to the static experiments performed at fixed depletion rate, the new approach enables to fully account for convective effects around the well. In terms of $K_r$, the results showed that strong differences exist with gas injection experiments. Non wetting phase is the more affected since $K_{rg}$ is several orders of magnitude lower than values derived from gas injection experiment. It means that gas mobility is sharply reduced when gas comes from solution. Significant differences also exist for $K_{ro}$. Higher values were obtained with solution gas. Both can be attributed to differences in phase distribution within the porous medium.

A pertinent value of $S_{gc}$ is also given by the dynamic experiments when gas mobility results from bubble connection. Interpretation is made through an analogy with experiments at fixed depletion rate. In both cases, a stabilized state is reached resulting from an equilibrium between diffusion and supersaturation and only the origin of this latter phenomenon differs. Hence, $S_{gc}$ value can be used straightforward by calculating an equivalent depletion rate.

In conclusion the new apparatus and methodology constitute a real improvement to measure, quickly, in one experiment all the parameters which play a role in flow behavior during solution gas drive process.

## ACKNOWLEDGEMENTS

The authors wish to thank S. Banini who performed the experiments. This work was funded by ARTEP (Association de Recherche sur les Techniques d'Exploitation du Pétrole) and

FSH (Fonds de Soutien des Hydrocarbures). The authors are grateful for permission to publish these results.

## NOMENCLATURE

| | | | |
|---|---|---|---|
| $C_o$ | : dissolute gas concentration | IFT | : interfacial tension |
| $\mu_o$ | : oil viscosity | $S_{gc}$ | : critical gas saturation |
| $Q_o$ | : oil injection rate | K | : absolute permeability |
| L | : core length | $K_{ro,g}$ | : oil, gas relative permeability |
| A | : core lateral area | $P^{th}_c$ | : threshold capillary pressure |
| U | : fluid velocity | $r_b$ | : bubble radius |
| $S_{wi}$ | : irreducible water saturation | $\varepsilon$ | : bubble minus outlet pressure |
| $P_b$ | : bubble pressure | $P_o$ | : outlet pressure |
| | | $\bar{r}$ | : average pore radius |

## REFERENCES


1 Stewart C.R. et al :'' The role of bubble gas limestones'', Trans AIME T.P. 3962, 17-20 Oct 1954, San Antonio.

2 Abgrall E., Iffly R. :'' Etude physique des écoulements par expansion des gaz dissous'', Revue de l'IFP, Vol 28, n°5, Sept-Oct 1973.

3 Moulu J-C., Longeron D. :'' Solution-Gas drive : experiments and simulation'', Fifth European Symposium on improved oil recovery, Budapest 1989.

4 Braithwaite C.I.M., Schulte W.M. :'' Transforming the future of the Brent Field : Depressurisation-The next developpement phase'', SPE 25026, European Petroleum conference, 16-18 November 1992, Cannes.

5 Christiansen S.H., Wilson P.M., :'' Challenges in the Brent field : implementation of depressurisation'', SPE 38469, Offshore Europe Conference, 9-12 Sept 1997, Aberdeen.

6 Kortekaas T.F.M., Van Poelgeest F. :'' Liberation of solution gas during pressure depletion of virgin and watered-out oil reservoirs'', SPE 19693, ATCE, 8-11 Oct 1989, San Antonio.

7 Scherpenisse W., Wit K. et al :'' Predicting gas saturation buildup during depressurisation of a North Sea oil reservoir'', SPE 28842, European Petroleum Conference, 25-27 Oct 1994, London.

8 Ligthelm D.J., Reijnen G.C.A.M. et al :'' Critical gas saturation during depressurisation and its importance in the Brent field'', SPE 38475, Offshore Europe Conference, 9-12 Sept 1997, Aberdeen.

9 Grattoni C.A., Hawes R.I., Dawe R.A.:" Relative permeabilities for the production of solution gas from waterflood residual oil", SCA n°9817, The Hague, 14-16 Sept 98.

10 Betata S.A. , Moulu J.-C. :'' Lab-to-field scaling of two-phase flow in the wellbore region'', SCA n°9806, The Hague 14-16 Sept 98.

11 Bourbiaux B. :'' Écoulements en abords des puits, perméabilités relatives en présence de gaz de solution'', Rapport IFP n°41096, 1994.

12 Chaumet P. , Cours de production, Tome 3, Editions Technip.

13 Tang G-Q., Firoozabadi A.:" Gas and liquid-phase ralative permeabilities for cold production from heavy oil reservoirs", SPE 56540, ATCE, 3-6 Oct 1999, Houston.

14 Kumar R., Pooladi-Darvish M.:"An investigation into enhanced recovery under solution gas drive in heavy oil reservoirs", SPE 59336, IOR Symp, 3-5 Apr 2000, Tulsa.